LETTERS

Metal saturation in the upper mantle

Arno Rohrbach[1,2], Chris Ballhaus[1], Ute Golla-Schindler[2], Peter Ulmer[3], Vadim S. Kamenetsky[4] & Dmitry V. Kuzmin[5,6]

The oxygen fugacity f_{O_2} of the Earth's mantle is one of the fundamental variables in mantle petrology. Through ferric–ferrous iron and carbon–hydrogen–oxygen equilibria, f_{O_2} influences the pressure–temperature positions of mantle solidi and compositions of small-degree mantle melts[1–3]. Among other parameters, f_{O_2} affects the water storage capacity and rheology of the mantle[4,5]. The uppermost mantle, as represented by samples and partial melts, is sufficiently oxidized to sustain volatiles, such as H_2O and CO_2, as well as carbonatitic melts[6,7], but it is not known whether the shallow mantle is representative of the entire upper mantle. Using high-pressure experiments, we show here that large parts of the asthenosphere are likely to be metal-saturated. We found that pyroxene and garnet synthesized at >7 GPa in equilibrium with metallic Fe can incorporate sufficient ferric iron that the mantle at >250 km depth is so reduced that an (Fe,Ni)-metal phase may be stable. Our results indicate that the oxidized nature of the upper mantle can no longer be regarded as being representative for the Earth's upper mantle as a whole and instead that oxidation is a shallow phenomenon restricted to an upper veneer only about 250 km in thickness.

Although at the time of core melt segregation the silicate Earth must have been highly reduced and in equilibrium with metallic iron, the Earth's upper mantle is now oxidized. Relative to the iron–wüstite reference, oxygen fugacities (f_{O_2}) recorded by upper-mantle rocks and mantle-derived melts range from 3 to 6 log units above the iron–wüstite equilibrium[8]. Equilibrium with (Fe,Ni) metal at the time of core formation would have afforded an f_{O_2} of about 2 log units below the iron–wüstite equilibrium[9]. Hence, shallow upper mantle seems to have experienced oxidation by 5 to 8 orders of magnitude in f_{O_2}.

In the shallow mantle, f_{O_2} is monitored by ferric–ferrous iron equilibria such as $6Fe_2SiO_4$ (in olivine) + $O_2 = 2Fe_3O_4$ (in spinel) + $3Fe_2Si_2O_6$ (in pyroxene) or $4Fe_2SiO_4$ (in olivine) + $Fe_2Si_2O_6$ (in pyroxene) + $O_2 = 2Fe^{2+}{}_3Fe^{3+}{}_2Si_3O_{12}$ (in garnet)[10–12]. f_{O_2} is dependent on bulk composition; the higher the Fe_2O_3/FeO bulk ratio, the more oxidized the respective mantle region will be. f_{O_2} is also pressure–temperature dependent. If at a given bulk Fe_2O_3/FeO, increasing pressure stabilizes phases that fractionate ferric iron (such as spinel or garnet), then the pressure will lower the activities of the Fe^{3+} components, causing reduction and superimposing on bulk compositional f_{O_2} effects a systematic, depth-related change in f_{O_2}. The general f_{O_2}–depth trend in the mantle is believed to be towards reduction[13,14].

To establish a redox profile through the upper mantle, we have equilibrated a model mantle composition (see Supplementary Information) in Fe-metal capsules to 14 GPa, corresponding to a depth of about 450 km. The starting composition was depleted relative to primitive mantle[15] by 30% in normative olivine and enriched in FeO to a molar Mg/(Mg+Fe) bulk ratio of 0.5, to stabilize ferric-iron-fractionating phases like pyroxene and garnet and to raise the iron detection limit for electron energy loss spectroscopy (EELS) analysis. Before experimentation, the starting composition was sintered at 1,150 °C in CO–CO_2 atmosphere at an f_{O_2} near iron–wüstite, to render it free of ferric iron. All experiments were performed in Fe-metal capsules from 1 to 14 GPa and 1,220 to 1,650 °C. The f_{O_2} at run conditions, ranging from 0.5 to 1.3 log units below the iron–wüstite equilibrium, was deduced from the FeO contents of pyroxene and garnet in equilibrium with metallic Fe, assuming ideal ionic solution models. Run products were analysed for major elements and then thinned to electron transparency. Pyroxene, garnet and majorite solid solutions were then analysed for their $Fe^{3+}/\Sigma Fe$ ratios using EELS[16,17].

At 1 GPa, stable silicate phases are olivine and two pyroxenes. From 3 to 6 GPa, subcalcic pyroxene coexists with garnet. In addition, all experimental charges are peppered with micrometre-sized metallic Fe grains (Fig. 1), suggesting that redox equilibrium with metallic Fe was attained. Al^{3+} in pyroxene falls with increasing pressure and modal garnet increases according to MAl_2SiO_6 (in clinopyroxene) + $M_2Si_2O_6$ (in clinopyroxene) = $M_3Al_2Si_3O_{12}$ (in garnet) where M =

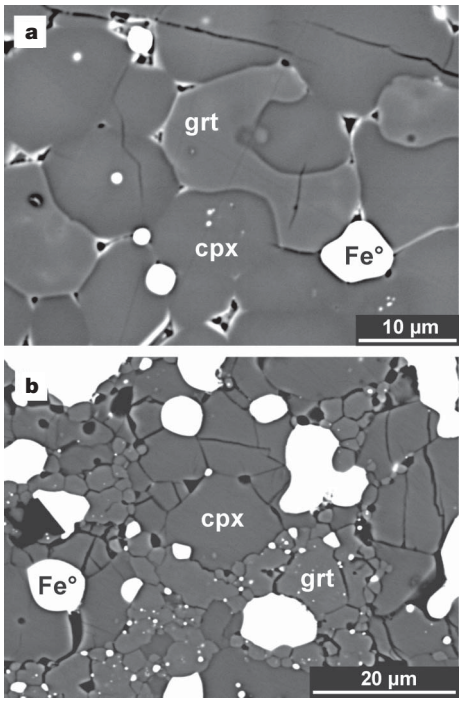

Figure 1 | Backscattered images of run products. a, 3 GPa experiment. **b**, 12 GPa experiment. Phases present are clinopyroxene (cpx), garnet (grt), metallic iron (Fe°) and minor amounts of partial melt.

[1]Mineralogisches-Petrologisches Institut und Museum, Universität Bonn, Poppelsdorfer Schloss, 53115 Bonn, Germany. [2]Institut für Mineralogie, Universität Münster, Corrensstrasse 24, 48149 Münster, Germany. [3]Institut für Mineralogie und Petrographie, ETH Zürich, Clausiusstrasse 25, 8092 Zürich, Switzerland. [4]ARC Centre of Excellence in Ore Deposits and School of Earth Sciences, University of Tasmania, Hobart, Tasmania 7001, Australia. [5]Max-Planck-Institut für Chemie, Abt. Kosmochemie, 55128 Mainz, Germany. [6]Institute of Geology and Mineralogy SB RAS, Novosibirsk 630090, Russia.

Mg^{2+}, Fe^{2+} and Ca^{2+} (Fig. 2a). At 7 GPa, pyroxene starts dissolving in garnet according to $2xM_2Si_2O_6$ (in clinopyroxene) + $M_3Al_2Si_3O_{12}$ (in garnet) = $[M_3Al_2Si_3O_{12}{\cdot}xM_3(MSi)Si_3O_{12}]$ (majorite$_{solid\text{-}solution}$) until in the highest-pressure run (14 GPa), majorite is the only crystalline silicate. Interestingly, the onset of majorite substitution is independent of bulk Mg/(Mg+Fe) and occurs at the same pressure as in the more magnesian bulk composition of ref. 18 (Fig. 2b).

Figure 3 shows pressure-dependent changes in $Fe^{3+}/\Sigma Fe$ in subcalcic pyroxene and garnet. Below 6 GPa, Fe^{3+} contents are pressure-insensitive but above 7 GPa, $Fe^{3+}/\Sigma Fe$ increase rapidly, up to 0.34 at 14 GPa. Generally, garnet has higher $Fe^{3+}/\Sigma Fe$ ratios than pyroxene, as in many natural garnet peridotites[19]. We note a stringent correlation of $Fe^{3+}/\Sigma Fe$ with majorite component in garnet (Fig. 4), expressed as a Si_{3+x} excess over stoichiometric garnet (for which the number of Si atoms is 3). Apparently, the ability of garnet to fractionate Fe^{3+} increases with majorite substitution.

We suggest that not only the lower mantle and the transition zone[13,14,20–23], but also the lower half of the upper mantle is metal-saturated. Fe-metal saturation will set in when the mantle silicates in equilibrium with metallic Fe can fractionate more Fe_2O_3 than is present in the fertile upper mantle. We can approximate the depth at which this is likely to happen. At 8 GPa, fertile mantle with 4.5 wt% Al_2O_3 and 3.7 wt% CaO (ref. 15) will crystallize about 20 wt% majoritic garnet, 15 wt% subcalcic clinopyroxene, and 65 wt% olivine (assuming all Al_2O_3 fractionates into garnet and all CaO into pyroxene). A typical iron content in garnet from garnet peridotite, calculated as FeO, is 8 to 10 wt% (refs 10, 19). In our 8 GPa garnets, 15 mol% of total Fe is ferric iron. Therefore, 20 wt% majoritic garnet with an average 9 wt% FeO (refs 10, 19) may fractionate about 2,400 p.p.m. Fe_2O_3, and this is in equilibrium with metallic Fe. Fertile upper mantle at shallow pressure contains about 2,000 p.p.m. Fe_2O_3 and about 8 wt% FeO (ref. 15). Hence, that same composition compressed to 7 to 8 GPa will be Fe-metal-saturated.

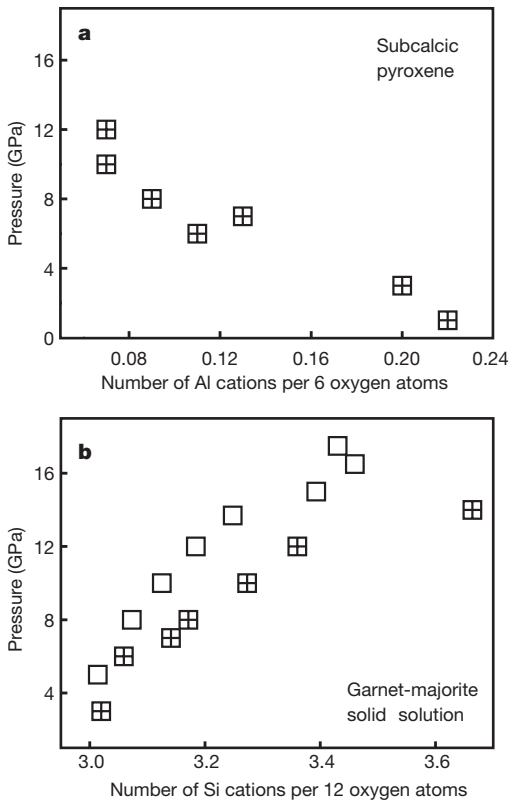

Figure 2 | Experimental clinopyroxene (a) and garnet–majorite compositions (b). Crossed symbols, this study (bulk Mg/(Mg+Fe) = 0.5); open symbols, ref. 18 with bulk Mg/(Mg+Fe) = 0.9. Onset of majorite substitution in garnet at about 7 GPa is independent of bulk Mg/(Mg+Fe).

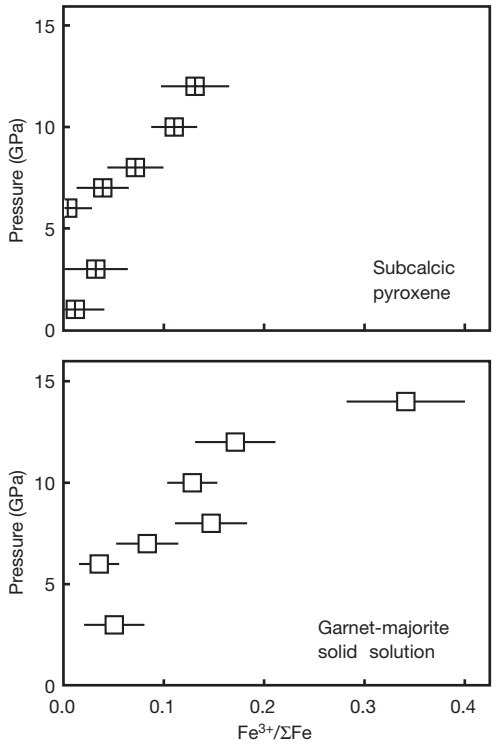

Figure 3 | Pressure effect on the $Fe^{3+}/\Sigma Fe$ atomic ratios of pyroxene and garnet (redox equilibrium with metallic Fe). Averages of 8 to 15 analyses per symbol. Error bars are standard errors of the mean with 95% confidence interval and include variations among analyses and uncertainties of the universal curve parameters of ref. 16.

Implicit in this calculation is that our FeO-enriched, olivine-depleted model composition correctly represents reactions among natural mantle phases. For example, if with increasing bulk FeO contents molar $Fe^{3+}/\Sigma Fe$ increased, as noted in ref. 24, we would have to correct our calculated level of metal saturation to greater depths because natural garnets are more magnesian. This does not seem to be the case, however. The garnets from the 8 GPa run and the 14 GPa run are the most magnesian (owing to some silicate melt lost from the charges), and yet they are within the $Fe^{3+}/\Sigma Fe$–pressure trend in Fig. 3b or even enriched in ferric iron (14 GPa). Also, we note that our calculation is generous in that it ignores the ferric iron fractionated by clinopyroxene (Fig. 3a), so the depth of metal saturation derived above is very realistic.

With metal saturation in the upper mantle, one could be inclined to interpret the chondritic highly siderophile element (HSE) and Os

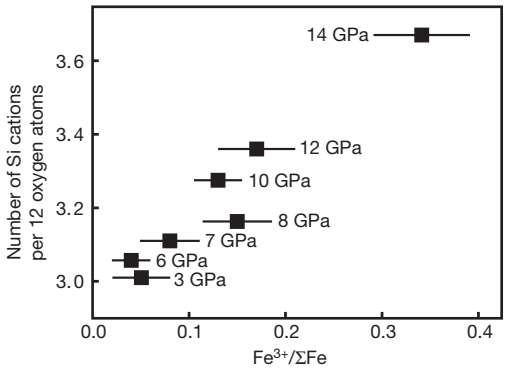

Figure 4 | Correlation between the $Fe^{3+}/\Sigma Fe$ atomic ratio and the Si_{3+x} excess in garnet–majorite solid solutions. Error bars are standard errors of the mean with 95% confidence interval and include variations among analyses and uncertainties of the universal curve parameters of ref. 16.

isotopic signatures[15,25,26] of the mantle in terms of a "ghost signature" of a stranded core melt fraction[27], stable at depth but oxidized during upward convection. The oxygen source would be Fe^{3+} derived from majorite breakdown. Assuming this is true, we could use the HSE abundances of the Earth's mantle and core[15] to broadly constrain, via mass balance, the amount of an (Fe,Ni)-metal phase at depth. This mass balance gives about 1,400 p.p.m. Fe metal. If we wanted to oxidize this amount of metal to FeO by majorite breakdown, to produce an HSE "ghost signature", we would require about 4,000 p.p.m. Fe_2O_3. This is about double the amount of Fe_2O_3 calculated above from majorite compositions. On this basis, it seems unlikely that metal saturation at depth is a relict from incomplete core formation. Also note that the upper mantle has Ni–Co overabundances[27], which in terms of absolute concentration, are more serious than the HSE overabundances. Basically, to account for the 2,370 p.p.m. NiO of the upper mantle by oxidation of a metal phase, in addition to the HSE overabundances, that metal would have to be nearly pure Ni, and this is quite unlike the composition of the outer core—unless the metal/silicate partition coefficients for Ni and Co decrease strongly with increasing pressure.

A metal phase at depth will influence petrologic processes in the upper mantle. In the presence of Fe-rich metal, a carbon–hydrogen–oxygen fluid will be CH_4–H_2 with negligible CO_2 and H_2O (ref. 6). Carbonates are presumably unstable[28] but if CH_4–H_2 fluids are decompressed they may react with Fe_2O_3 released by majorite breakdown to CO_2 and H_2O, lowering the melting temperature and inducing redox melting[1]. The low-velocity region under mid-ocean ridges, which ref. 3 related to incipient $CO_2 \pm H_2O$-triggered melting, may coincide with the depth level at which we expect a metal phase to become unstable, that is, at which carbon–hydrogen–oxygen speciations would be shifted from CH_4–H_2 to H_2O–CO_2 and induce small-degree melting. Metal saturation may also limit the amount of water to be stored in nominally anhydrous minerals because carbon–hydrogen–oxygen fluids in equilibrium with metallic Fe will be H_2O-poor[6]. Clearly, experiments are needed to test the water-storage capacity of nominally anhydrous minerals under Fe-metal-saturated conditions with CH_4–H_2 fluid.

Is there independent evidence from natural samples for a highly reduced upper mantle? In garnet peridotite xenoliths a continuous decline in relative f_{O_2} has been noted[14] with increasing pressure to 6 GPa. Clearly, a shallow mantle trend towards reduction is encouraging for metal precipitation at greater depths. Direct evidence for metal saturation comes from Fe metal and Fe_xC carbide inclusions in diamonds[29,30], but one may speculate whether such inclusions record ambient f_{O_2} mantle conditions or local, short-lived redox perturbations when these diamonds grew[29]. Primitive mantle melts from metal saturation depths (>250 km) seem to be rare (see also Supplementary Information). Either the necessary depths are not normally tapped or deep mantle melting itself is oxidizing, that is, triggered by oxidation[1]. We note, however, that recently reported kimberlites are reduced as much as 5 log units below the nickel–NiO buffer, which is not far from (Fe,Ni)-metal saturation[31,32].

Received 12 March; accepted 8 August 2007.

1. Taylor, W. R. & Green, D. H. in *Magmatic Processes: Physicochemical Principles* (ed. Mysen, B. O.) 121–138 (Geochemical Society USA Special Publication 1, University Park, Pennsylvania, 1987).
2. Ballhaus, C., Berry, R. F. & Green, D. H. Oxygen fugacity controls in the Earth's upper mantle. *Nature* **348,** 437–440 (1990).
3. Dasgupta, R. & Hirschmann, M. M. Melting in the Earth's deep upper mantle caused by carbon dioxide. *Nature* **440,** 659–662 (2006).
4. Kohlstedt, D. L., Keppler, H. & Rubie, D. C. Solubility of water in the alpha, beta and gamma phases of $(Mg,Fe)_2SiO_4$. *Contrib. Mineral. Petrol.* **123,** 345–357 (1996).
5. Keppler, H. & Rauch, M. Water solubility in nominally anhydrous minerals measured by FTIR and 1H MAS NMR; the effect of sample preparation. *Phys. Chem. Miner.* **27,** 371–376 (2000).
6. Matveev, S., Ballhaus, C., Fricke, K., Trunckenbrodt, J. & Ziegenbein, D. CHO volatiles under upper mantle conditions. I. Experimental results. *Geochim. Cosmochim. Acta* **61,** 3081–3088 (1997).
7. Wallace, M. E. & Green, D. H. An experimental determination of primary carbonatite magma composition. *Nature* **335,** 343–346 (1988).
8. Frost, B. R. in *Oxide Minerals; Petrologic and Magnetic Significance* (ed. Lindsley, D. H.) 1–9 *Reviews in Mineralogy* (ed. Ribbe, P. H.) Vol. 25 (Mineralogical Society of America, Washington DC, 1991).
9. O'Neill, H. St. C. The origin of the Moon and the early history of the Earth – A chemical model. Part 2: The Earth. *Geochim. Cosmochim. Acta* **55,** 1159–1172 (1991).
10. Luth, R. W., Virgo, D., Boyd, F. R. & Wood, B. J. Ferric iron in mantle-derived garnets. *Contrib. Mineral. Petrol.* **104,** 56–72 (1990).
11. Ballhaus, C., Berry, R. F. & Green, D. H. Experimental calibration of the olivine–orthopyroxene–spinel oxygen barometer—implications for oxygen fugacity in the Earth's upper mantle. *Contrib. Mineral. Petrol.* **107,** 27–40 (1991).
12. Wood, B. J., Bryndzia, L. T. & Johnson, K. E. Mantle oxidation state and its relationship to tectonic environment and fluid speciation. *Science* **248,** 337–345 (1990).
13. Ballhaus, C. Is the upper mantle metal-saturated? *Earth Planet. Sci. Lett.* **132,** 75–86 (1995).
14. Woodland, A. B. & Koch, M. Variation in the oxygen fugacity with depth in the upper mantle beneath the Kaapvaal craton, Southern Africa. *Earth Planet. Sci. Lett.* **214,** 295–310 (2003).
15. Palme, H. & O'Neill, H. St. C. in *The Mantle and Core* (ed. Carlson, R. W.) 1–38 *Treatise on Geochemistry* (eds Holland, H. D. & Turekian K. K.) Vol. 2 (Elsevier–Pergamon, Oxford, 2003).
16. van Aken, P. A. & Liebscher, B. Quantification of ferrous/ferric ratios in minerals: new evaluation schemes of Fe L_{23} electron energy-loss near-edge spectra. *Phys. Chem. Miner.* **29,** 188–200 (2002).
17. van Aken, P. A., Liebscher, B. & Styrsa, V. J. Quantitative determination of iron oxidation states in minerals using Fe $L_{2,3}$-edge electron energy-loss near-edge structure spectroscopy. *Phys. Chem. Miner.* **25,** 323–327 (1998).
18. Irifune, T. An experimental investigation of the pyroxene–garnet transformation in a pyrolite composition and its bearing on the constitution of the mantle. *Phys. Earth Planet. Inter.* **45,** 324–336 (1987).
19. Canil, D. & O'Neill, H. St C. Distribution of ferric iron in some upper-mantle assemblages. *J. Petrol.* **37,** 609–635 (1996).
20. O'Neill, H. St C. *et al.* Mössbauer spectroscopy of mantle transition zone phases and determination of minimum Fe^{3+} content. *Am. Mineral.* **78,** 456–460 (1993).
21. Frost, D. J. *et al.* Experimental evidence for the existence of iron-rich metal in the Earth's lower mantle. *Nature* **428,** 409–412 (2004).
22. Wade, J. & Wood, B. J. Core formation and the oxidation state of the Earth. *Earth Planet. Sci. Lett.* **236,** 78–95 (2005).
23. Sinmyo, R., Hirose, K., O'Neill, H. St. C. & Okunishi, E. Ferric iron in Al-bearing post-perovskite. *Geophys. Res. Lett.* **33,** L12S13, doi:10.1029/2006GL025858 (2006).
24. McCammon, C. A. & Ross, N. L. Crystal chemistry of ferric iron in $(Mg,Fe)(Si,Al)O_3$ majorite with implications for the transition zone. *Phys. Chem. Miner.* **30,** 206–216 (2003).
25. Ringwood, A. E. Origin of chondrites. *Nature* **207,** 701–704 (1965).
26. Meisel, T., Walker, R. J. & Morgan, J. W. The osmium isotopic composition of the Earth's primitive upper mantle. *Nature* **383,** 517–520 (1996).
27. Jones, J. H. & Drake, M. J. Geochemical constraints on core formation in the Earth. *Nature* **322,** 221–228 (1986).
28. Eggler, D. H. & Baker, D. R. in *High Pressure Research in Geophysics* (eds Akimoto, S. & Manghnani, M. H.) 237–250 (Center Academic, Tokyo, 1982).
29. Jacobs, D. E., Kronz, A. & Viljoen, K. S. Cohenite, native iron and troilite inclusions in garnets from polycrystalline diamond aggregates. *Contrib. Mineral. Petrol.* **146,** 566–576 (2004).
30. Stachel, T., Harris, J. W. & Brey, G. P. Rare and unusual mineral inclusions in diamonds from Mwadui, Tanzania. *Contrib. Mineral. Petrol.* **132,** 34–47 (1998).
31. Bellis, A. J. & Canil, D. Ferric iron in $CaTiO_3$ perovskite as an oxygen barometer for kimberlitic magmas. I: Experimental calibration. *J. Petrol.* **48,** 219–230 (2007).
32. Canil, D. & Bellis, A. J. Ferric iron in $CaTiO_3$ perovskite as an oxygen barometer for kimberlite magmas. II: Applications. *J. Petrol.* **48,** 231–252 (2007).

Supplementary Information is linked to the online version of the paper at www.nature.com/nature.

Acknowledgements We thank the Museum of Natural History in London for providing Karoo picrite samples from Malawi. Comments on the manuscript by R. Frost and D. Canil and D. Frost improved the paper. Financial support by the German Research Council to C.B. is gratefully acknowledged.

Author Information Reprints and permissions information is available at www.nature.com/reprints. Correspondence and requests for materials should be addressed to A.R. (rohrbaa@web.de) or C.B. (ballhaus@uni-bonn.de).

SUPPLEMENTARY DISCUSSION

It is possible that melts from (Fe,Ni) metal–saturated sources can be recognized by their olivine compositions. Out of all transition metal oxides in olivine, NiO is most easily reduced to metal when fO_2 falls, followed by CoO and FeO. The sequence of reduction follows broadly the electromotive series. Therefore, a melt that is generated in equilibrium with an (Fe,Ni) metal phase may contain olivines that have unusually low NiO concentrations at slightly lower CoO and FeO. Examples are olivines from lunar basalts[33,34] and olivines from melts that experienced reduction because they became contaminated with organic carbon[35]. Suppl. Fig. S1 summarizes compositions of olivine phenocrysts from two samples of Karoo picrites from southern Malawi[36]. The majority of grains have normal to high NiO concentrations around 3500 ppm, and Ni/Co ratios of 18 to 20. Both NiO and Ni/Co show the usual decline in concentration with increasing fayalite (Fe_2SiO_4) component, consistent with a magmatic differentiation trend. The cores of some primitive olivines, however, have NiO concentrations as low as 300 ppm and Ni/Co atomic ratios of ~ 5, defining what is termed in Suppl. Fig. S1a an oxidation trend. Usually, low–NiO compositions are only preserved in cores of phenocrysts, and they are overgrown by rims rich in NiO and slightly enriched in CoO and FeO. Obviously, if metal–saturated conditions were responsible they could have prevailed only in the very early stages of melt generation. No metal inclusions have yet been identified in these olivines, so the ultimate test for our proposal of metal saturation still is missing. None the less, low NiO and Ni/Co at slightly lowered fayalite are signatures expected with metal saturation. It might be worthwhile in future to analyze more systematically olivine populations in primitive melts generated at great depths, to test how widespread these signatures are and whether they correlate with the depth of melting.

33. Karner, J., Papike, J. J. & Shearer, C. K. Olivine from planetary basalts; chemical signatures that indicate planetary parentage and those that record igneous setting and process. *Am. Mineral.* **88**, 806–816 (2003).
34. Papike, J. J., Fowler, G. W., Adcock, C. T, & Shearer, C. K. Systematics of Ni and Co in olivine from planetary melt systems: Lunar mare basalts. *Am. Mineral.* **84**, 392–399 (1999).
35. Pedersen A. K. Basaltic glass with hightemperature equilibrated immiscible sulphide bodies with native iron from Disko, central west Greenland. *Contrib. Mineral. Petrol.* **69**, 397–407 (1979).
36. Woolley, A. R., Bevan, J. C., Elliott, C. J. The Karroo dolerites of southern Malawi and their regional geochemical implications. *Mineral. Mag.* **43**, 487–495 (1979).
37. Sobolev A. V., et al. Estimating the amount of recycled crust in sources of mantle-derived melts. *Science* **316**, 412–417 (2007).

Figure S1

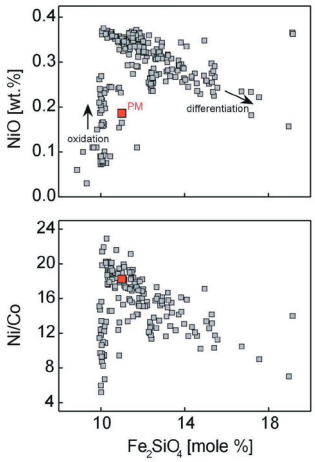

Figure S1: NiO contents and Ni/Co atomic ratios of olivines in the Karoo picrite sample P23-9 (ref. 35). Superimposed a putative metal oxidation trend (i.e., increasing NiO and Ni/Co at constant FeO) followed by a magmatic differentiation trend. Primitive mantle (PM) values are taken from Palme & O'Neill[15]. Analyses with the JEOL JXA– 8200 Superprobe at Max Planck Institute for Chemistry in Mainz, with some additional Ni analyses performed at the University of Cologne. Analytical conditions were 20 kV/300 nA with 120 sec on peak and background[37].

Table S1: Starting composition and representative electron microprobe analyses of run products.

		exp-10	exp-15	exp-15	zuII-4	zuII-4	zuIII-1	zuIII-1	zu-8	zu-8	zuII-3	zuII-3	zuIV-1	zuIV-1	zuIII-4
pressure (GPa)		1	3	3	6	6	7	7	8	8	10	10	12	12	14
temperature (°C)		1220	1400	1400	1400	1400	1450	1450	1650	1650	1500	1500	1500	1500	1500
run time (h)		48	24	24	4.5	4.5	6	6	1.5	1.5	3.5	3.5	10	10	4.5
ΔfO_2 (IW)		- 0.6(3)	- 0.5(3)	- 0.5(3)	- 0.5(3)	- 0.5(3)	- 0.6(3)	- 0.6(3)	- 1.1(3)	- 1.1(3)	- 0.7(1)	- 0.7(1)	-0.7(2)	-0.7(2)	- 1.3(3)
phase	start. comp.	cpx	grt	cpx	grt	cpx	grt	cpx	grt	cpx	grt	cpx	grt	cpx	grt
SiO_2	47.5	48.8	39.4	50.6	40.4	52.3	40.6	51.8	43.9	54.8	43.5	52.3	43.8	52.7	50.5
TiO_2	0.29	0.18	0.56	0.28	0.81	0.20	0.70	0.23	0.40	0.11	0.68	0.16	0.46	0.16	0.36
Al_2O_3	6.45	4.76	21.2	4.38	20.7	2.45	18.3	2.78	18.1	2.12	15.2	1.50	14.0	1.63	8.40
Cr_2O_3	0.56	0.74	1.30	0.50	1.26	0.36	1.02	0.34	0.96	0.27	0.87	0.29	1.10	0.33	0.69
FeO[a]	26.2	26.4	23.6	24.0	25.0	26.5	23.4	22.7	13.7	13.1	22.1	23.5	20.3	19.7	9.77
Fe_2O_3[a]	–	0.3	1.38	0.82	1.16	0.09	2.26	1.05	2.68	1.10	3.67	3.23	4.61	3.26	5.59
MgO	14.7	13.5	9.21	14.2	9.93	14.9	11.4	15.3	18.4	21.5	12.9	15.6	12.4	15.3	19.4
CaO	3.80	6.01	4.01	4.10	3.82	4.34	3.10	4.43	3.41	6.44	2.91	4.46	2.72	5.11	5.25
Na_2O	0.50	0.16	0.03	0.85	0.04	0.67	0.16	1.18	0.19	1.01	0.14	0.74	0.32	1.15	1.56
Total	100.0	100.9	100.7	99.7	102.0	101.8	100.9	99.8	101.7	100.5	102.0	101.8	99.7	99.3	101.5
Mg/(Mg+Fe)[a]	0.5	0.48(1)	0.41(1)	0.51(1)	0.41(1)	0.50(1)	0.47(1)	0.55(1)	0.71(3)	0.75(2)	0.51(3)	0.54(2)	0.52(1)	0.58(1)	0.78(2)
$Fe^{3+}/\Sigma Fe$ (EELS)		0.01(3)	0.05(3)	0.03(3)	0.04(2)	0.00(3)	0.08(3)	0.04(3)	0.15(4)	0.07(3)	0.13(2)	0.11(3)	0.17(5)	0.13(4)	0.34(6)
Si (per formula unit)		1.88(1)	3.01(1)	1.93(2)	3.06(2)	1.98(1)	3.11(2)	1.97(1)	3.18(2)	2.00(1)	3.28(2)	1.99(1)	3.36(2)	2.02(1)	3.67(1)
Al (per formula unit)		0.22(2)	1.91(2)	0.20(2)	1.76(2)	0.11(1)	1.65(4)	0.13(1)	1.55(2)	0.09(1)	1.35(3)	0.07(1)	1.27(1)	0.07(1)	0.72(3)

Uncertainties in parenthesis are standard errors of the mean (95% confidence). (a) Recalculated based on $Fe^{3+}/\Sigma Fe$ ratio (EELS). Electron microprobe analyses at 15 kV and 15 nA using natural silicates as standards. Run products were thinned to electron transparency with a Gatan Duo-Mill ion milling system. Pyroxene, garnet, and majorite$_{ss}$ were analyzed for $Fe^{3+}/\Sigma Fe$ ratios with a Zeiss Libra 200 FE transmission electron microscope equipped with an in-column Omega energy filter and operated at 200 kV. The energy resolution was about 1 eV, measured as full width at half maximum of the zero loss peak. Molar $Fe^{3+}/\Sigma Fe$ was calculated from the iron $L_{2/3}$ spectra using the calibration of van Aken & Liebscher[16]. Background subtraction followed the procedure described by van Aken et al.[17]. fO_2 values calculated from ferrosilite (in cpx) and almandine (in grt) activities using ideal ionic solution models. Note that the 8 GPa and 14 GPa runs may have suffered some melt loss at run conditions, causing silicates to be more magnesian and Mg/(Mg+Fe) atomic ratios more variable. In the high pressure runs > 8 GPa some chemical variation may also be owed to the small amount of starting material (~ 5 mg) that can be equilibrated (c.f. elevated sodium content in grt at 14 GPa).